BBAA VI International Colloquium on:
Bluff Bodies Aerodynamics & Applications
Milano, Italy, July, 20–24 2008

STATIC RESPONSE COEFFICIENTS FROM DYNAMIC CABLE-MODEL TESTS

Terje L. Andersen[⋆] **and Jasna B. Jakobsen**[⋆]

[⋆]Department of Mechanical and Structural Engineering and Material Science
University of Stavanger, 4036 Stavanger, Norway
e-mails: Terje.L.Andersen@UiS.no, Jasna.B.Jakobsen@UiS.no

Keywords: Circular cable, Dry cable response, Static coefficients, Dynamic tests, Drag crisis, Drag coefficient model.

Abstract: *The present paper summarises static mean response coefficients from dynamic cable model tests, carried out in the critical Reynolds number range. Response data is obtained from an elastically supported cable section model with full scale diameter for typical bridge stay cables (160mm). The tests were performed at the National Research Council (NRC), Canada in 2001. The analysis covers a total of 337 recorded time series of wind excited response in the region of critical Reynolds number. Dynamic tests was performed at three different inclinations to the mean-wind velocity vector i.e. inclination: $35°$, $45°$ and $60°$ in wind flows of $10 - 38m/s$.*

The coefficients obtained are compared to force coefficients from surface pressure data from static scale-model tests performed at NRC in 2002. Surface pressure data from fixed model tests cover the interval of equivalent inclinations from $55°$ to $90°$. Wind velocities in the range $20 - 100m/s$ reproduce similar wind conditions as for the dynamic tests.

Static coefficients are presented based on the wind-flow component normal to the inclined cable axis as normal coefficient C_N and cross-flow lift coefficient C_L.

The commonly applied ESDU recommendations for two-dimensional flow is compared to available data. For the general three-dimensional flow conditions around inclined cylinders, an alternative expression for the drag normal coefficients throughout the critical Reynolds number range is presented. The suggested expression uses 7 parameters to fit coefficients both from static surface pressure tests and dynamic response tests with good accuracy during the drag-crisis transition.

1 INTRODUCTION

Wind induced vibrations of inclined circular cylinders have been observed for high reduced wind velocities, both on bridge stay cables and in wind tunnel tests with an elastically supported sectional model of a stay-cable [2]. The large response occurs in the region of critical Reynolds number wind-flow conditions, also called *drag-crisis*. It is evident that low eigen-frequency and -damping are paramount to the development of large vibrations, and increased damping can suppress the vibrations [7, 8]. The actual interaction mechanism between flow and structure, causing the dynamic response, is however not completely understood at present.

While the dynamic response is the main interest and concern for structures utilizing cables, the static response is equally important for the understanding of the flow-structure interaction. This paper focuses on the averaged "static" force coefficients associated with variable magnitudes of dynamic response.

Load coefficients from fixed-cylinder surface pressure data is used as a reference for comparison [4, 6].

ESDU recommendations [3] are commonly used to define an analytical approximation of the drag coefficients on circular cylinders in perpendicular and angled flow conditions. The ESDU recommendation is however quite hesitant especially with respect to the effect of inclined cylinders with different surface conditions in the critical Reynolds number region. This paper presents results from a large number of tests, and in addition suggests a drag coefficient expression as function of Reynolds number, capable of reproducing the general shape of the C_N curve in the drag crisis region.

2 CABLE MODEL CHARACTERISTICS

The cable model is a spring supported steel pipe and HDPE cover with outside diameter $D = 160mm$. Spring supports are placed in two orthogonal directions perpendicular to the cable axis (*sway* and *heave*). Model inclination, ϕ, is adjustable. See table 1 for details of test setups. The dynamic cable model is confined to the same vertical plane in all tests. However, the cable and spring supports can be rotated (α) in order to simulate skew alignment of prototype cable to natural wind. Different levels of damping are introduced. Damping is highly dependent of the response amplitude. The primary translation vibration modes of the cable model have slightly detuned natural frequencies around $f_{\text{sway}} \approx f_{\text{heave}} \approx 1.4Hz \pm 3\%$. The dynamic tests

Case	Setup	ϕ	α	Surface	Damping
1	1B	$45.0°$	$0.0°$	smooth	low
2	1B	··	··	smooth	very high
3	1B	··	··	smooth	interm.
4	1B	··	··	smooth	high
5	1B	··	··	rough	low
6	1C	$45.0°$	$54.7°$	rough	low
7	1C	··	··	smooth	low
8	2C	$60.0°$	$54.7°$	smooth	low
9	2C	··	··	smooth	very high
10	2A	$60.0°$	$0.0°$	smooth	low
11	2A	··	··	smooth	high
12	2A	··	··	smooth	high
13	2A	··	··	smooth	vertical
14	2A	··	··	rough	vertical
15	2A	··	··	rough	low
16	3A	$35.0°$	$0.0°$	rough	low
17	3A	··	··	smooth	low
18	3B	$35.0°$	$58.7°$	smooth	low

Table 1: Parameters for test cases. *Vertical* damping denotes setups with high damping in heave, and low damping in sway. *Smooth* is the original clean surface condition of the HDPE material. *Rough* surface is obtained with spray-glue and contaminations of dust etc. Approx. damping relative to critical at dynamic response standard deviation of approx. 5% of cable diameter: *low*; 0.03%, *intermediate*; 0.06%, *high*; 0.24% and *very high*; 0.6% [2].

were performed at three angles of incidence between wind and cable axis: $\phi = 35°$, $\phi = 45°$ and $\phi = 60°$.

3 DYNAMIC RESPONSE

The large dynamic responses observed during tests is the prime interest for investigation. Two types of responses are categorized as: *dry inclined cable galloping response* in case 8 and *high-speed vortex excitation* in case 10 [2]. Both incidences occurred in close proximity to the drag crisis. Maximum dynamic responses for all test cases can be divided into two groups: $Re_{ESDU} \approx 4.4 \cdot 10^5$ and $Re_{ESDU} \geq 5.7 \cdot 10^5$. Both Reynolds number ranges correspond to the boundary layer transition regimes TrBL1-3, according to the notation suggested by Zdravkovich [9].

4 STATIC COEFFICIENTS

The dynamic time series are here used to establish time averaged *static coefficients*. The raw data available is recorded deflections along spring support directions at the cable model ends. The centre point deflections in sway (s) and heave (h), perpendicular to the cable axis are determined as the mean of the corresponding end deflection, see eq. (1). In the initial position of the model (no rotation of spring supports) heave is parallel to normal component of wind flow on cable and sway is perpendicular to both wind flow and cable, see figure 1. For rotated spring supports the lift- and normal drag deflections, y and z are calculated by the transformation given in eq. (2).

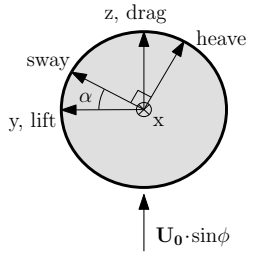

Figure 1: Cross section of cable with definition of reference coordinates and spring support rotation angle, α.

$$\begin{bmatrix} s \\ h \end{bmatrix} = \frac{1}{2} \cdot \left(\begin{bmatrix} s \\ h \end{bmatrix}_{top} + \begin{bmatrix} s \\ h \end{bmatrix}_{bottom} \right) \quad (1)$$

$$\begin{bmatrix} y \\ z \end{bmatrix} = \begin{bmatrix} \cos\alpha & -\sin\alpha \\ \sin\alpha & \cos\alpha \end{bmatrix} \cdot \begin{bmatrix} s \\ h \end{bmatrix} \quad (2)$$

$$q_0 = \frac{1}{2} \cdot \rho \cdot (U_0 \cdot \sin\phi)^2 \quad (3)$$

$$z_0 = \frac{q_0 \cdot D \cdot L}{K} \quad (4)$$

$$C_N = \frac{\overline{z}}{z_0} \ , \ C_L = \frac{\overline{y}}{z_0} \quad (5)$$

At a given tunnel wind-velocity U_0, the wind pressure normal to cable axis is defined from eq. (3). Air density is $\rho = 1.25 kg/m^3$. The static reference deflection, z_0, perpendicular to cable in the cable-wind plane is established from the base pressure, cable diameter, wind exposed length of cable (here assumed to be L) and translational stiffness ($K = 31.5 kN/m$) ref. eq. (4). Coefficients for the normal drag and transverse lift are then established as the ratio of time averaged deflections $\overline{y}$ and $\overline{z}$ relative to the reference deflection ref. eq. (5). The coefficients represent the total load on the cylinder. The information is thus averaged both in time and along the model dimension. The coefficients are further a measure of the combined effects of surface pressure C_{Np} and surface friction C_{Nf} [9, (1.2)]:

$$C_N = C_{Np} + C_{Nf} \quad (6)$$

For comparison to the static coefficients from dynamic tests, surface pressure data from a test series performed at the NRCC in 2002 are re-visited [6]. These tests have been discussed by Macdonald & Larose [7, 8] in terms of the associated aerodynamic damping, relevant for development of large cable response. The surface pressure recordings give information about the static *surface pressure coefficients* C_{Np} *locally* at the individual circumferential rings of pressure taps (32 taps per ring).

The coefficients are presented with respect to Reynolds number $\mathrm{Re} = U_0 \cdot D/\nu$. Kinetic viscosity of air is $\nu = 1.5 \cdot 10^{-5} m^2/s$. Both dynamic- and surface pressure test series cover the critical Reynolds number range with flow-transition characterised by significant reduction in drag (drag crisis). The ESDU correction for wind turbulence (λ_T), and cylinder surface roughness (λ_R) and non-perpendicular incidence angle ϕ, given in eq. (7) is applied to the data [3]. In the present paper, all tested surface conditions are in practice considered to be smooth (i.e. $\lambda_R = 1$). The wind tunnel flow turbulence in the two different tests are approximately $I_u = \frac{\sigma_u}{U_0} = 0.75\%$ in the dynamic tests, and $I_u = 0.14\%$ in the static tests.

$$Re_{ESDU} = \lambda_T \cdot \lambda_R \cdot \frac{U_0 D}{\nu} \cdot \frac{1}{\sin\phi} \tag{7}$$

5 STATIC RESPONSE

The main feature of the static mean response is the drag crisis characterised by a sharp drop of normal drag, see figure 2 for static coefficients in all cases (on figure 2 and subsequent figures the largest responses for each case is accentuated with stars and large circles). The onset of drag crisis is denoted critical Reynolds number. ESDU defines critical Reynolds number for perpendicular flow drag coefficient (C_{D0}): "In general, Re_{crit} is the value of Re at which C_{D0} falls to a value of 0.8..." [3]. This suggests a $1/3$ decrease of the initial $C_{D0} = 1.2$ pre-critical plateau.

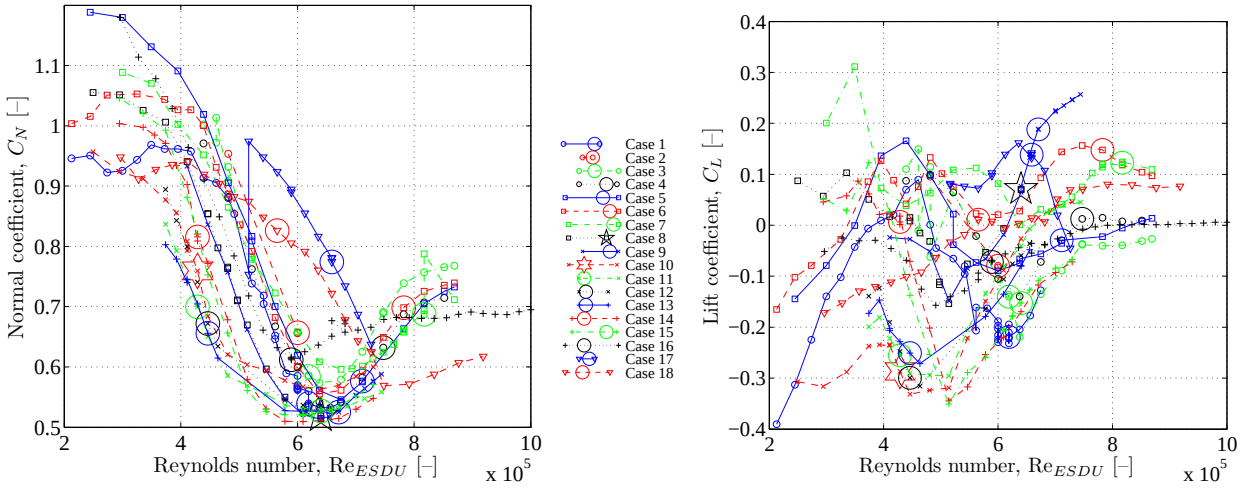

(a) Static normal drag coefficients.

(b) Static Lift coefficients.

Figure 2: Static coefficients for all dynamic cable tests. Note that the largest dynamic responses for each case is accentuated with stars and large circles.

Figure 3a shows setups with angle of incidence $\phi = 60°$. The cases include six with smooth surface and two with slightly rougher surfaces (all considered smooth in the Reynolds number

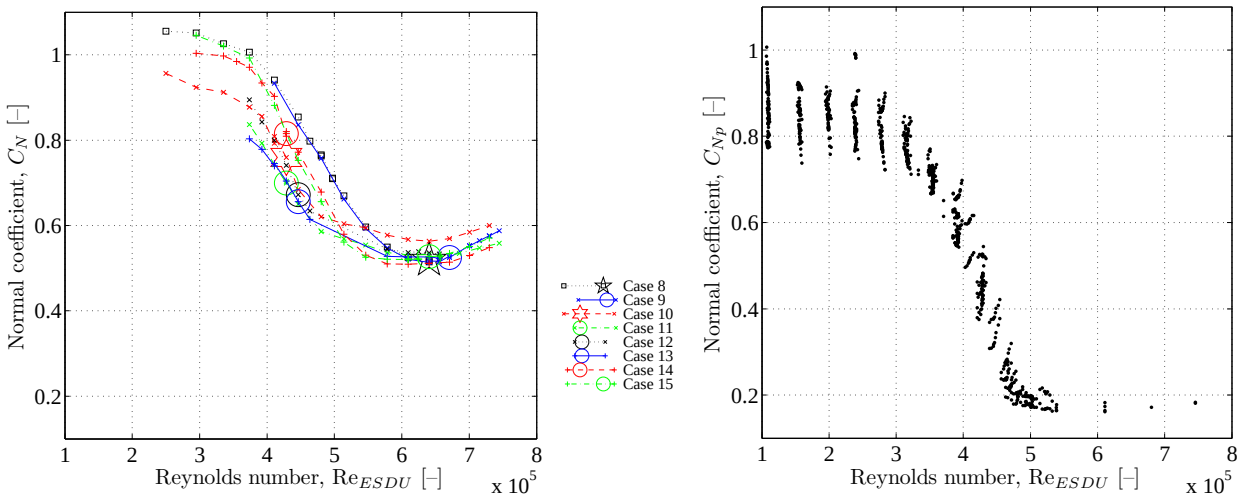

(a) Normal drag.

(b) Normal pressure drag.

Figure 3: Static coefficients for cases with angle of incidence $\phi = 60°$. (a) Dynamic test results. (b) Surface pressure results for range $\phi = 60° \pm 2°$ for rings number 2 and 4 in the central part of the tested cylinder.

adjustment). Figure 3b shows the corresponding coefficients from surface pressure data for $\phi \approx 60°$. The normal drag graphs all have a similar trend. Assuming that a reduction to $2/3$ of drag coefficient plateau prior to drag crisis is a valid measure to define critical Reynolds number, then both test series indicate a critical Reynolds number; $\mathrm{Re}_{crit} \sim 4.0 \cdot 10^5 - 5 \cdot 10^5$. Comparing the graphs from dynamic- and surface pressure tests on figures 3a and 3b, there is a systematic difference in the magnitude of the coefficients and in the post critical shape of the curves: The total normal drag coefficients from dynamic test show a local minimum of C_N after the drag crisis. C_{Np} on the other hands appears to reach a constant level immediately after the drag crisis. According to Zdravkovich, C_{Nf} in eq. (6) becomes negligible beyond shear layer transition (TrSL) at $\mathrm{Re} \approx 2 \cdot 10^5$ [9]. Based on this, a good agreement between C_N and C_{Np} could be expected in the investigated Reynolds number range. The difference in the coefficient values may thus not be affiliated with friction, but can in parts be ascribed to modelling differences between the two tests, such as tunnel blockage, end effects etc. An important difference between the two test series is the total load on full model length vs. local pressure load at specific model cross section. Zdravkovich describes a wide scatter of C_N values in the post critical *TrBL3* regime and links it to either 1) a preserved two-bubble formation similar to *TrBL2* yielding low C_N or 2) fragmentation of bubbles linked to increased C_N level [9]. The few available data points on figure 3b may be in any of these two bubble conditions e.g. with preserved bubbles and low C_{Np}. The length-averaged coefficients on figure 3a, can be expected to contain a combination of both bubble conditions or possibly a fully fragmented bubble state and due to this show a higher post critical drag level. The overall larger coefficients on figure 3a than those on figure 3b may obviously also indicate that the movement of the cable and the associated fluid-structure interaction contribute to overall drag.

6 DRAG-COEFFICIENT FIT

An analytical expression for measured drag coefficients in drag crisis transition is suggested in the following. The expression is devised to represent overall characteristic of the drag coefficient change during drag crisis. The main transition from high to low C_N is represented by one term, $C_1(\mathrm{Re})$. The effect of local minimum drag at the end of the transition is described by $C_2(\mathrm{Re})$. The expression in (10) is entirely based on the normal distribution: C_1 is a scaled version of the *complementary error function* and C_2 is a scaled *Gaussian probability density function*. In addition to good fitting properties the smooth expression is also well conditioned for application to numerical as well as analytical models.

$$C_1(\mathrm{Re}) = \frac{C_0 - C_\infty}{\sqrt{\pi}} \int_{\mathrm{Re}}^{\infty} e^{-\left(\frac{x-\mu_1}{\sigma_1}\right)^2} dx \tag{8}$$

$$C_2(\mathrm{Re}) = C_\delta \cdot e^{-\frac{1}{2}\cdot\left(\frac{Re-\mu_2}{\sigma_2}\right)^2} \tag{9}$$

$$C_N(\mathrm{Re}) \approx C_1(\mathrm{Re}) - C_2(\mathrm{Re}) + C_\infty \quad , \quad \mathrm{Re} \in [100k; 1M[\tag{10}$$

The approximation in (10) is a 7-parameter model: C_0 is the initial pre-critical C_N-plateau value. C_∞ is the post-critical C_N-plateau value. The main transition takes place symmetrically around a critical Reynolds number value $\mathrm{Re}_{cr} = \mu_1$ with a transition range defined by the standard deviation variable $\Delta\,\mathrm{Re} = \sigma_1$. C_δ is the correction applied to C_N at the Reynolds number $\mathrm{Re} = \mu_2$. The extend of local minimum correction is defined by the standard deviation variable $\Delta\,\mathrm{Re} = \sigma_2$. Based on the available data, the limits of the fit is defined as Reynolds numbers in the range 100k to 1M. This range covers shear layer burst to turbulence (TrSL3), precritical- one-bubble– and two-bubble– boundary layer transitions (TRBL0–2) and parts of the supercritical boundary layer transition regime (TrBL3) as defined by Zdravkovich [9].

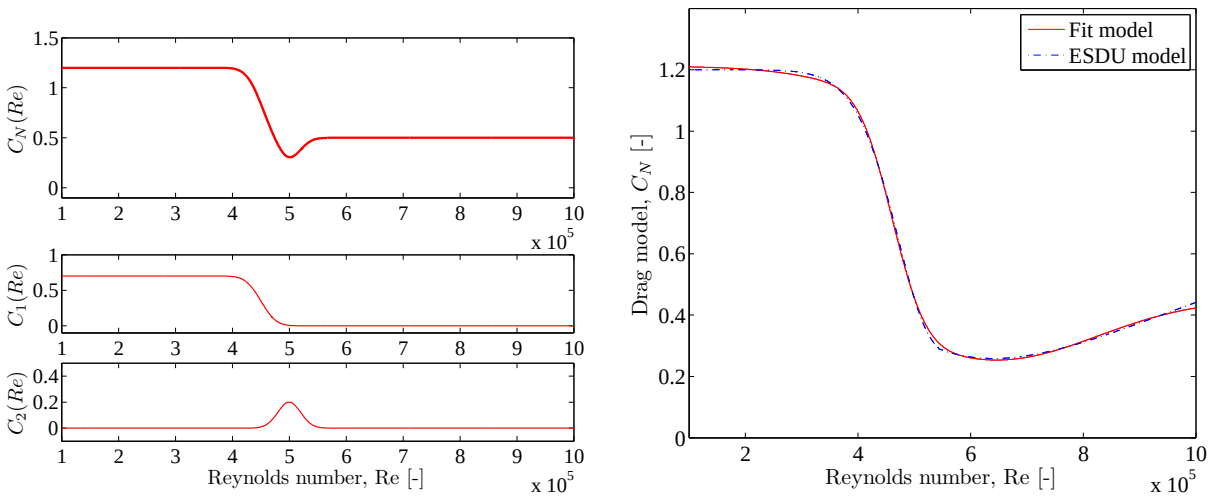

(a) Drag fit model.

(b) Fit to ESDU model.

Figure 4: 7-parameter model for drag coefficient in the critical Reynolds number range. (a) Individual terms of fitting model eq. (10), illustrated with $C_0 = 1.20$, $C_\infty = 0.50$, $\mu_1 = 4.50 \cdot 10^5$, $\sigma_1 = 0.3 \cdot 10^5$, $C_\delta = 0.20$, $\mu_2 = 5.50 \cdot 10^5$ & $\sigma_2 = 0.20 \cdot 10^5$. (b) Drag coefficient fit to obtain the ESDU reference curve for two-dimensional flow $\phi = 90°$ [3, C1.1–C1.4f]. (parameters for the fit are listed in table 4).

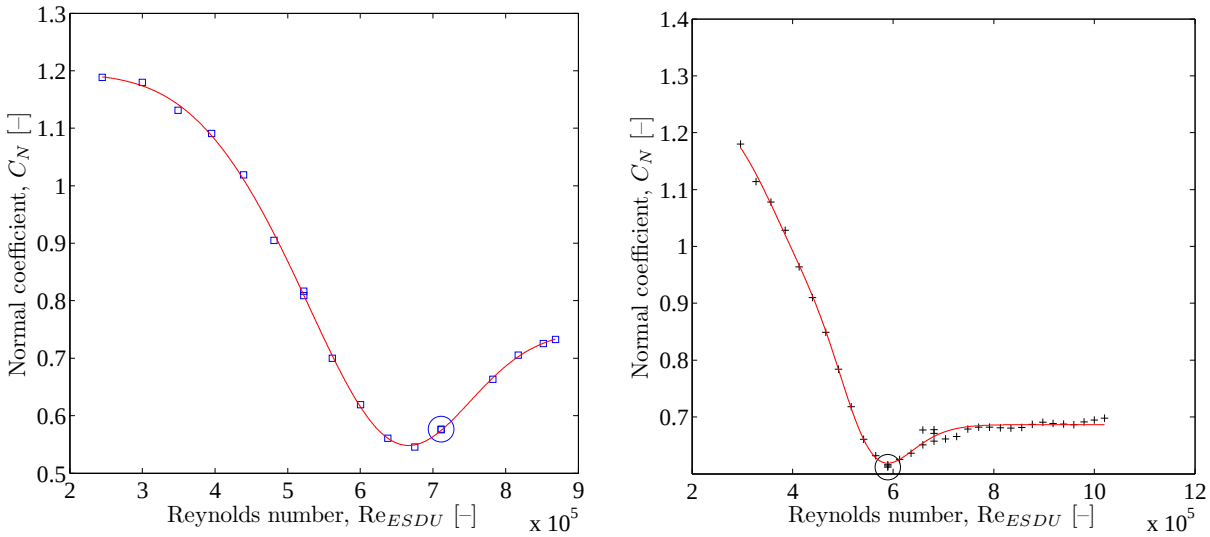

(a) Case 5. (b) Case 16.

Figure 5: 7-parameter model applied to two individual test cases from dynamic cable tests. (a) *Case 5* drag coefficient fit, $\phi = 45°$. (b) *Case 16* drag coefficient fit, $\phi = 35°$. (Parameters for both fits are listed in table 3).

The individual parts of the fit approximation are illustrated on figure 4a. Figure 4b shows that the fitting model is capable of reproducing the overall shape of the ESDU reference curve for two-dimensional flow ($\phi = 90°$) with smooth cylinder surface ($\epsilon/D = 0$) as defined in [3, C1.1–C1.4f]. The primary defining parameters for the ESDU curve are $\mathrm{Re}_{eA} = 5.43 \cdot 10^5$ and $\mathrm{Re}_{eB} = 7.33 \cdot 10^5$. Due to the different approach, the comparable parameters for the fit model are $0.82 \cdot 10^5$ and $0.87 \cdot 10^5$ lower respectively at $\mu_1 = 4.61$ and $\mu_2 = 6.46$. Note that the fit model parameter, μ_1, is very close to the EDSDU definition of critical Reynolds number $\mathrm{Re}_{crit} = 4.5 \cdot 10^5$.

Figure 5 shows fits of results from two of the dynamic test cases. The quality of the fits are representative for all 18 data cases, except case 2 and 17. In case 2 too few data points are available for fitting. In case 17 too little data is available to establish either of the asymptotic parameters C_0 and C_∞, these two plateau values for the drag coefficient are essential for obtaining good fit parameters. Thus a wide span of data, as e.g. Case 5 on figure 5a will produce good coefficients. Although fits like case 16 on figure 5b also produce visually good fits, the parameters for e.g. the initial C_0 plateau may not reflect true conditions. The actual fitting operation is performed in Matlab using the fit-toolbox and a non-linear least-squares optimization. In situations where the pre- (C_0) and post-critical (C_∞) drag coefficients are not well defined from the tests, limits to the parameters must be applied. All fits are performed with sets of initial- and limit-parameters as listed in table 2.

6.1 Fit of dynamic test coefficients

Table 3 include parameters for drag coefficient fit of individual test cases. The table also include collective fits of all tests at angles of wind-cable incidence of $\phi = 45°$ and $\phi = 60°$. The $\phi = 45°$ approximation is shown on figure 6a. Corresponding lift coefficients are plotted on figure 6b where the first derivative of the drag coefficient fit ($dC_N(\mathrm{Re})/d\,\mathrm{Re}$) is also plotted. A similar set of graphs are presented on figure 7 for the $\phi = 60°$ data. It is evident that the $C_N(\mathrm{Re})$

	C_0 [–]	C_∞ [–]	μ_1 [$\cdot 10^5$]	σ_1 [$\cdot 10^5$]	C_δ [–]	μ_2 [$\cdot 10^5$]	σ_2 [$\cdot 10^5$]
Low limit	0.7	C_{min}	2.0	0.05	0.0	3.0	0.0
Dynamic seed	1.1	0.7	5.0	3.0	0.6	7.2	2.0
Static seed	1.2	0.4	4.0	3.0	0.05	5.0	1.0
High limit	$2 \cdot C_{max}$	1.0	7.0	7.0	1.0	10.0	∞

Table 2: Parameter limits and initial seed value for least square fitting of dynamic model response drag coefficients and static model surface pressure drag coefficients. C_{min} and C_{max} is smallest respectively largest coefficient values in actual data to be fitted, assuming that data cover the drag crisis.

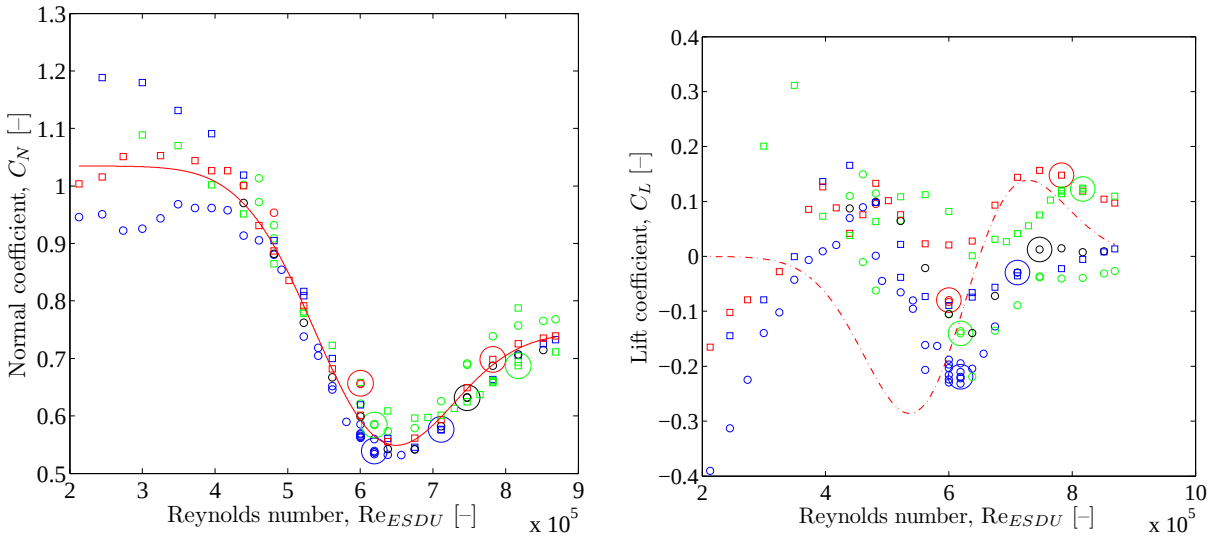

(a) Normal drag.

(b) Lift.

Figure 6: Normal force coefficients from dynamic model tests with angle of incidence $\phi = 45°$. (a) shows normal drag coefficients and least square fit for all tests combined (ref. table 3 for parameters of the fit). (b) shows corresponding lift coefficients. Also plotted on (b) is the first derivative of the C_N fit: Dash-dot line is $\frac{dC_N(\mathrm{Re})}{d\,\mathrm{Re}} \cdot 10^5$.

approximations produce good estimates in the critical and post critical Reynolds number region. The pre-critical data for especially the $\phi = 45°$ test cases are more dispersed.

The Lift coefficient data on figures 6b and 7b are apparently not well organized, but some relation to the change of drag coefficient might be considered, so that $dC_N(\mathrm{Re})/d\,\mathrm{Re}$ gives a qualitative progression of the static lift, but in no way a complete description. The drag derivative $dC_N(\mathrm{Re})/d\,\mathrm{Re}$ does reproduce the change of sign of C_L observed in several of the $\phi = 45°$ cases. For the $\phi = 60°$ cases, there seems to be a quite close relation including a translation along the Re-axis, so that $C_L(\mathrm{Re}_0) \propto dC_N(\mathrm{Re})/d\,\mathrm{Re}|_{\mathrm{Re}=\mathrm{Re}_0 - \mathrm{Re}_1}$, with $\mathrm{Re}_1 = 0.5 - 1.0 \cdot 10^5$, ref figure 8.

With respect to any linkage between static coefficients and largest dynamic response (indicated by large circle- and star- symbols on figures) one clear observation can be made: Large responses in the Reynolds number range $\mathrm{Re} \approx 4.4 \cdot 10^5$ for $\phi = 60°$ clearly coincide quite closely with largest change of C_D, and the mean lift is non-zero in the majority of cases. This group of large responses include the case 10 *high-speed vortex excitation*. The other group of dynamic responses at $\mathrm{Re} > 5.7 \cdot 10^5$ for both $\phi = 45°$ and $\phi = 60°$ are more scattered with respect to static coefficients: For $\phi = 45°$ the largest responses seem to occur adjacent to, but

Case no.	Inclination ϕ [°]	C_0 [–]	C_∞ [–]	μ_1 [$\cdot 10^5$]	σ_1 [$\cdot 10^5$]	C_δ [–]	μ_2 [$\cdot 10^5$]	σ_2 [$\cdot 10^5$]	
1	45	0.95	0.55	5.95	0.52	0.23	5.58	0.51	
2	··	–	–	–	–	–	–	–	
3	··	1.22	0.64	6.99	3.96	0.41	6.21	1.05	
4	··	1.38	0.54	5.40	6.69	0.35	6.31	1.04	
5	··	1.20	0.75	4.70	1.45	0.21	6.56	0.92	(fig. 5a)
6	··	1.04	0.74	6.55	0.64	0.41	6.04	0.84	
7	··	1.10	0.75	4.51	1.10	0.16	6.83	0.83	
1–7	45	1.03	0.75	6.23	1.33	0.33	6.16	0.95	(fig. 6)
8	60	1.06	0.62	6.16	0.88	0.40	5.53	0.90	
9	··	1.16	0.71	4.99	1.47	0.27	5.69	1.42	
10	··	0.99	0.82	4.27	0.36	0.25	6.28	1.99	
11	··	1.02	0.83	4.19	0.52	0.30	6.36	2.45	
12	··	1.19	0.88	4.25	0.59	0.34	6.94	4.52	
13	··	0.85	0.53	4.34	0.74	0.00	6.24	5.86	
14	··	1.01	0.58	4.42	0.77	0.08	6.16	0.89	
15	··	1.39	0.80	4.45	0.87	0.34	3.38	4.71	
8–15	60	1.03	0.86	3.93	0.58	0.34	6.40	1.46	(fig. 7)
16	35	1.26	0.69	5.13	0.79	0.29	4.55	0.99	(fig. 5b)
17	··	–	–	–	–	–	–	–	
18	··	0.94	0.61	6.21	1.78	0.09	7.63	0.58	
16–18	35	–	–	–	–	–	–	–	

Table 3: Parameters for drag coefficient fit of dynamic test cases. Cases 2 & 17 has too few points to accommodate satisfactory fitting. The two available data cases 16 & 18 for $\phi = 35°$ are too different to produce a reasonable common fit for the inclination.

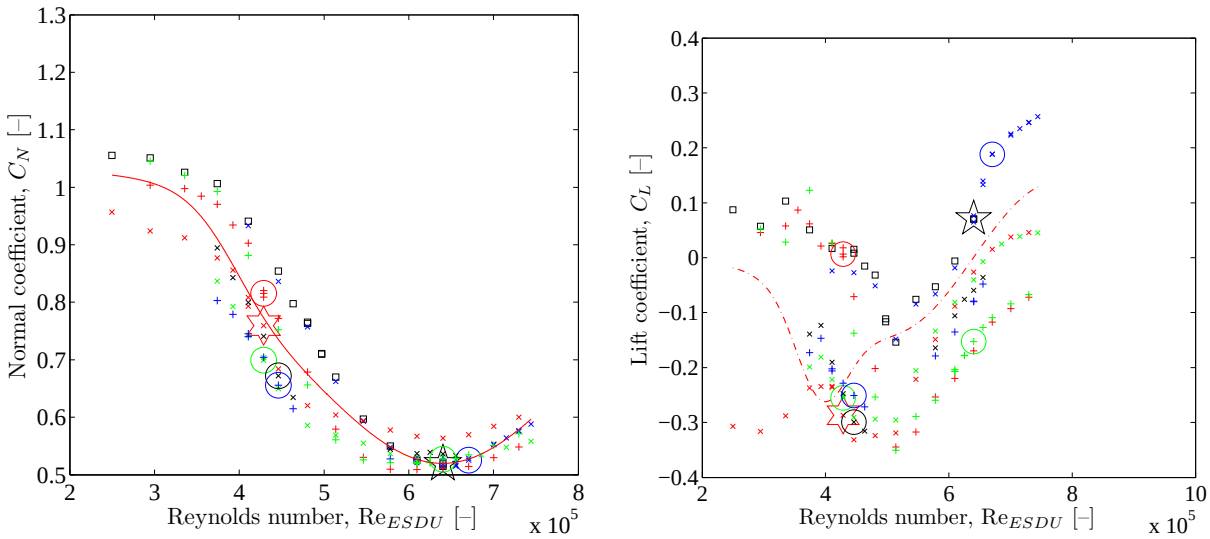

(a) Normal drag.

(b) Lift.

Figure 7: Normal force coefficients from dynamic model tests. All tests with angle of incidence $\phi = 60°$.

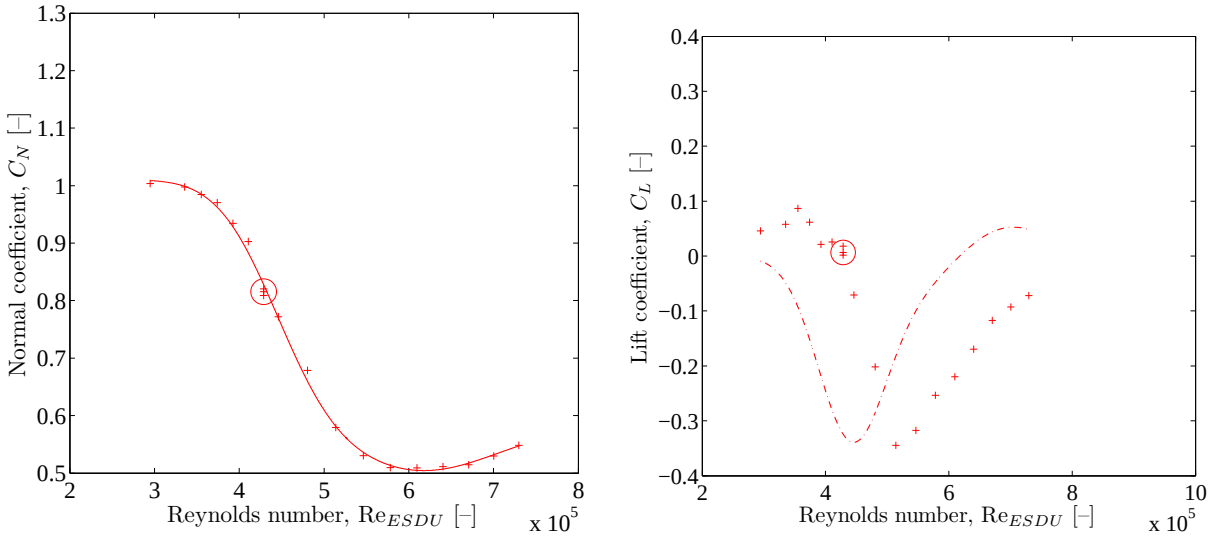

(a) Normal drag. (b) Lift.

Figure 8: Normal force coefficients from dynamic model test case no. 14.

not at, the actual minimum drag. On the other hand, the largest responses at $\phi = 60°$ seems to occur at the minimum value of C_D. The latter group includes the response termed *dry inclined cable galloping response* in the previous study [2].

The force coefficients interpreted from mean response of the cable model suggest that the large vibration events take place at wind speeds associated with rapid changes in normal drag coefficient, and a non-zero value of the lift coefficient in many cases. For an increasing wind speed, these situations may correspond to flow oscillations between a no bubble and one bubble flow regime, and between one bubble and two bubble regimes, as the flow patterns are about to establish more coherently along the inclined model. In [4], an example of a lift coefficient time-history varying between no bubble and a single bubble regime, on a section of the fixed cable model, is given. In [5], a simulation of a dynamic cable response based on such load records indicated that they might initiate a large cable response.

A comprehensive analysis of cable response in two degrees of freedom based on mean load coefficients was carried out in [7, 8], suggesting that certain episodes of large response can be attributed to a complex variation of mean load coefficients with Reynolds number and cable orientation. It is expected that expressions such as eq. (10) can be of benefit to future modelling for prediction of large vibrations occurring at the drag-crisis flow transition in the critical Reynolds-number range. Generic parameters for the 7 fitting parameters may to some extend be derived from the results included in tables 3 and 4 and more application specific data is easily fitted if required. A significant benefit of the parametric expression (10) is the smoothness of the function which makes it adoptable for numeric evaluation.

6.2 Fit of Surface pressure coefficients

The C_N fitting model eq. (10) is also applied to the static surface pressure data. In table 4, fitting parameters are presented for several angles of inclination to wind. The $\phi = 90°$ situation is plotted on figure 9. On the figure, the ESDU reference situation is also shown [3, C1.1–C1.4f]. Except for a translation along the Reynolds number axis, the data, fitted curve and ESDU graphs follow reasonably. While the ESDU definition of critical Reynolds number is $\mathrm{Re}_{crit} = 4.5 \cdot 10^5$, the data suggests $\mathrm{Re}_{cr} \approx \mu_1 = 3.49 \cdot 10^5$ with the ESDU correction of

Inclination ϕ [°]	C_0 [–]	C_∞ [–]	μ_1 [$\cdot 10^5$]	σ_1 [$\cdot 10^5$]	C_δ [–]	μ_2 [$\cdot 10^5$]	σ_2 [$\cdot 10^5$]	
55	0.75	0.18	4.66	1.45	0.14	5.20	0.32	
60	0.85	0.16	4.26	1.34	0.15	4.82	0.34	(fig. 10)
65	1.13	0.37	4.01	4.69	0.51	4.62	0.56	
70	1.18	0.88	2.23	0.74	0.70	4.45	0.56	
75	1.18	0.91	2.38	0.50	0.74	4.30	0.51	
82	1.26	0.24	3.75	2.31	0.44	4.13	0.33	
90	1.27	0.31	3.49	1.50	0.26	4.26	0.41	(fig. 9)
ESDU 90	1.21	0.45	4.61	0.64	0.20	6.46	1.80	(fig. 4b & 9a)

Table 4: Parameters for drag coefficient fit of static surface pressure tests obtained from available data in range $\phi \pm 1°$. Note that the lag of sufficient data in the post critical Reynolds range affects the quality of the fits. The best established fits for inclinations $\phi = 60°$ and $\phi = 90°$ are plotted in figures 10 and 9.

wind turbulence incorporating, without any surface roughness correction, ref. eq. (7).

Figure 10 represents the only actual overlap of data between dynamic and static tests: The $\phi = 60°$ pre-critical surface pressure coefficient C_0 is reduced by approx. $1/3$ with respect to the perpendicular flow conditions on figure 9. The post-critical plateau C_∞ is similarly reduced by approx. 50%. Comparing figure 10a with 7a, the surface pressure coefficient (C_{Np}) is also observed to be significantly lower than the total drag coefficients (C_N) at identical inclination. The relative pre-critical difference between C_N and C_{Np} according to the fitted expressions is 17% and the post-critical is 81%. The difference is much more pronounced in the post critical range, as discussed in relation to figure 3 on page 5.

The treatment of cylinder inclination to flow in ESDU [3] includes separate sub– and super–critical adjustments to the basic $90°$ situation plotted on figure 9. The ESDU corrections are among other data sets based on the investigations by Bursnall and Loftin [1]. A general agreement between the surface pressure data presented in the present paper and the summarizing figure in Bursnall and Loftin report is quite clear [1, fig. 9]: The Bursnall and Loftin data for inclinations $\phi = 30° - 90°$[1] presents C_D at $\mathrm{Re} = 2.0 \cdot 10^5$ in the range 1.0–1.3, and post-critical at $\mathrm{Re} = 4.0 \cdot 10^5$ in the range 0.2–0.75. Comparing these values with the fit parameters C_0 : 0.75–1.27 and C_∞ : 0.18–0.91 the similarity is quite reasonable. The surface pressure data is thus considered in good agreement with the established reference cases applied through the ESDU recommendations.

While drag coefficients are lower, the lift coefficients from the surface pressure data on the other hand appears to be larger than the corresponding lift coefficients from dynamic tests. Since pressure data concern local flow conditions, as opposed to spatially averaged data from dynamic tests, and there is a considerable variation of local lift coefficients along the model, in the critical Reynolds number range, it is plausible that local lift coefficients from surface pressure data are larger than those from the dynamic tests. Another important difference between the two tests is motion, and it is considered likely that the deviation for both coefficients can be, at least partially, attributed to the structural motion and resulting change to flow caused by interactions between wind load and structural response.

[1] Note opposed angle definition in [1]

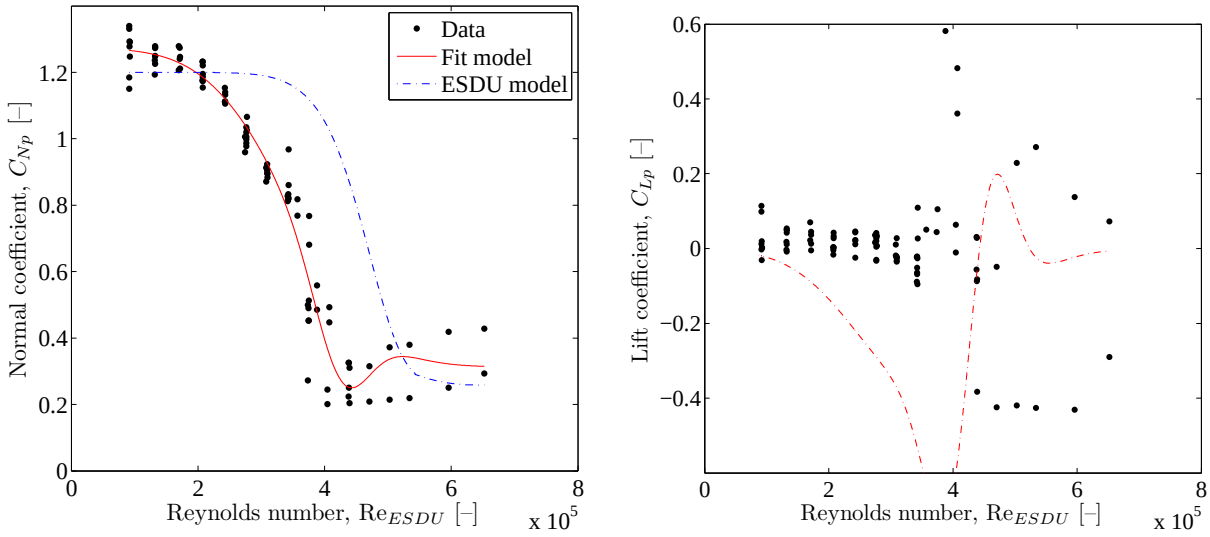

(a) Normal pressure drag.

(b) Pressure lift.

Figure 9: Pressure coefficients from static surface pressure tests. All tested angles of incidence in range $\phi = 90° \pm 1°$. Results for two locations of pressure tap rings are shown (rings 2 and 4). (a): Drag coefficient data (points), fit (full line) and ESDU reference graph (dash–dot). (b): Lift coefficient data (points) and first derivative of drag-coefficient-fit (dash–dot).

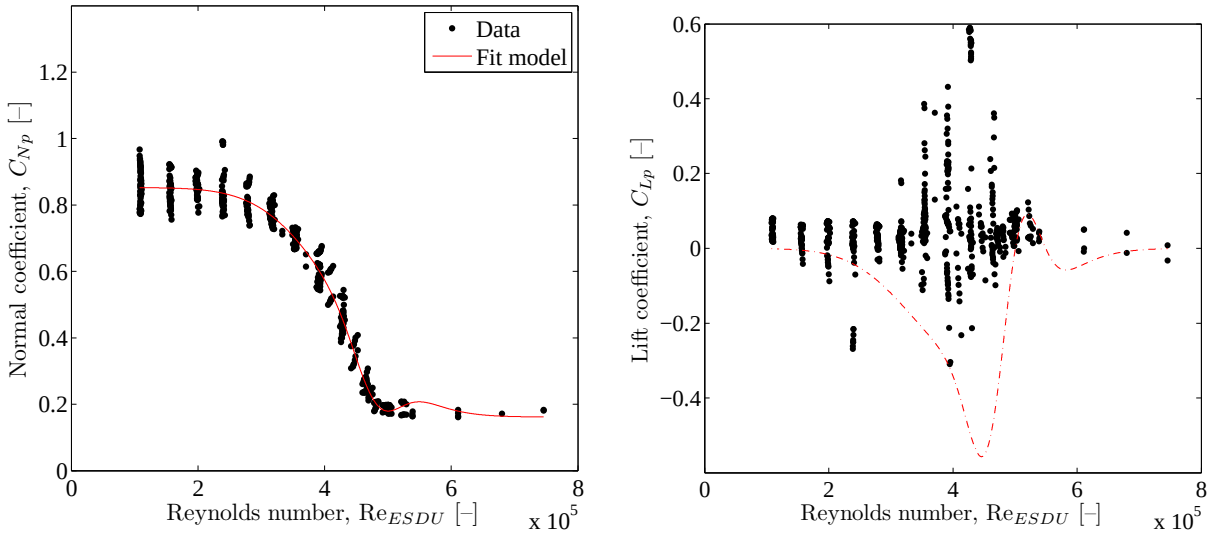

(a) Normal pressure drag.

(b) Pressure lift.

Figure 10: Pressure coefficients from static surface pressure tests. All tested angles of incidence in range $\phi = 60° \pm 1°$. Results for two locations of pressure tap rings are shown (rings 2 and 4).

7 CONCLUSION

Dynamic cable model response recorded for inclined cable in the critical Reynolds number range is studied in terms of the associated static forces coefficients. Displacement time-series are translated to normal drag- and lift coefficients, as functions of effective Reynolds number. Events of large dynamic cable response are observed to take place at large changes of drag coefficient or in the vicinity of the post-crisis low-point of drag coefficient. A considerable fraction of the dynamic events appear to be associated with a non-zero mean lift coefficient.

The static coefficients obtained from dynamic tests are compared to coefficients deduced from surface pressure measurements on a fixed cable model. It is observed that the surface pressure coefficients are in good agreement with earlier reference data, but significantly lower than comparable ones from the dynamic response tests, especially in the post-critical Reynolds number range.

With engineering practice commonly linked to drag coefficients based on surface pressure recordings, it is important to note that the present data suggests that larger time-averaged loads than anticipated could be the result of structural vibrations. In order to quantify the change of drag coefficient throughout the *drag-crisis* or *critical Reynolds number range*, a 7-parameter expression is suggested. The parameters are all linked to the shape of the general drag coefficient curve in a straight forward way. The suggested expression for the C_N coefficient produces a smooth curve without dis-continuities, applicable for numerical evaluation. The drag coefficient expression is fitted to the available test data producing a series of parameter-sets covering wind-cylinder incidence angles from $\phi = 55^\circ$ to 90° for surface pressures tests, and angles $\phi = 45^\circ$ and 60° for dynamic test.

In order to distinguish different flow regimes and ultimately predict conditions susceptible to large response, it is important to gain a better understanding of all aspects of flow and structure interaction, not least the time-averaged response treated in the present paper.

ACKNOWLEDGEMENTS

The authors wish to thank everybody at National Research Council, Canada — Institute for Aerospace Research — Aerodynamics Laboratory, especially leader of the Bluff-Body Aerodynamics group, Dr. Guy L. Larose for a most welcoming co-operation on the research of circular cylinder aerodynamics.

REFERENCES

[1] W. J. Bursnall and L. K. Loftin, Jr. *Experimental investigations of the pressure distribution about a yawed circular cylinder in the critical Reynolds number range*. NACA Technical Note 2463, Langley, Sept. 1951.

[2] S. Cheng, G. L. Larose, M. G. Savage and H. Tanaka. Aerodynamic behaviour of an inclined circular cylinder. *Wind & Structures*, **6**(3):197–208, 2003.

[3] ESDU 80025. *Mean forces, pressures and flow field velocities for circular cylindrical structures*. Oct. 1980.

[4] J. B. Jakobsen, G. L. Larose and M. G. Savage. *Instantaneous Wind Forces on Inclined Circular Cylinders in Critical Reynolds Number Range*. Proc. 11th Int. Conf. on Wind Engineering, Lubbock, TX, USA, June 2nd-5th, 2003.

[5] J. B. Jakobsen, T. L. Andersen and G. L. Larose. *Interpretation of Wind Forces Monitored on an Inclined Stationary Cylinder in Critical Reynolds Number Range in Relation to Observed Aeroelastic Model Response*. Proc. Sixth Int. Symp. on Cable Dynamics, Charleston, SC, USA, Sept. 19th–22nd, 2005

[6] G. L. Larose, M. G. Savage and J. B. Jakobsen. *Wind tunnel experiments on an inclined and yawed circular cylinder in the critical Reynolds number range*. Proc. 11th Int. Conf. on Wind Engineering, Lubbock, TX, USA, June 2nd-5th, 2003.

[7] J. H. G. Macdonald and G. L. Larose. *Two-degree-of-freedom inclined cable galloping–Part 1: General formulation and solution for perfectly tuned system*. JWEIA 96 (2008) 291–307.

[8] J. H. G. Macdonald and G. L. Larose. *Two-degree-of-freedom inclined cable galloping–Part 2: Analysis and prevention for arbitrary frequency ratio*. JWEIA 96 (2008) 308–326.

[9] M. M. Zdravkovich. *Flow Around Circular Cylinders 1: Fundamentals*. Oxford University Press, 1997.